Journal of Alloys and Compounds 489 (2010) 451–455

Contents lists available at ScienceDirect

Journal of Alloys and Compounds

journal homepage: www.elsevier.com/locate/jallcom

Influence of the Nd^{3+} ions content on the FTIR and the visible up-conversion luminescence properties of nano-structure $BaTiO_3$, prepared by sol–gel technique

A.G.A. Darwish[a], Y. Badr[b], M. El Shaarawy[c], N.M.H. Shash[c], I.K. Battisha[a,*]

[a] National Research Center (NRC), Department of Solid State Physics, Cairo, Egypt
[b] National Institute of Laser Enhancement Sciences (NILES), Cairo University, Egypt
[c] Physics Department, Faculty of Science, Banha University, Egypt

ARTICLE INFO

Article history:
Received 1 May 2009
Received in revised form 3 September 2009
Accepted 6 September 2009
Available online 11 September 2009

Keywords:
Sol–gel
Powders
Up-conversion
$BaTiO_3$ nano-crystals
XRD
FTIR and Nd^{3+} ions

ABSTRACT

The nano-structure $BaTiO_3$ (BT) powder doped with different concentrations of Nd^{3+} ions were annealed at 750 °C for 1 h to form nano-structure tetragonal phase of BT powder. The structure properties studied using XRD and FTIR methods. Sensitized up-conversion luminescence observed under excitation of 808 nm diode laser, suggesting that the Nd^{3+} ions-doped BT might be an ideal up-conversion material for infrared excitation. The influence of increasing the concentration of the Nd^{3+} ions on the luminescence intensity investigated using laser diode. The up-conversion mechanisms in the doped system will be discussed by analyzing the energy level structures of the Nd^{3+} ions.

1. Introduction

During the past few decades there have been considerable interests in the up-conversion of phosphors; much of the early work aimed at producing up-conversion lamp and all solid-state lasers [30]. In recent years, there has been a renewed interest in the RE ions-doped up-conversion materials due to their practical applications such as IR laser detecting, laser ant forgery and biomedicine diagnosis [1,2], and their potential applications such as solid-state display [3], fiber optic amplifiers [4]. The rare earth RE doped solids as for other fluorescence light emitters usually follow the well-known principle of the Stokes law which simply states that excitation photons are at higher energy than emitted ones, or in other words that out put photon energy is weak, less than input photon energy. For the "unconventional case", called up-conversion the above principle is not respect and the emission found to exceed excitation energies, so the up-conversion process defined as a non-linear optical process in which the light frequency is increased. The up-conversion process has three principal mechanisms by which it accomplished; these are multi-photon absorption, cooperative energy-transfer up-conversion, and the photon avalanche, Fig. 1 as indicated previously [5].

Some sol–gel procedures have been developed by using a mixture of alkoxides and barium carbonate, with the synthesis of a pure cubic and tetragonal phases being achieved upon a final temperature treatment of 800 °C. Despite the high cost of the precursors, the sol–gel procedure became attractive for advanced nano-structure ceramics preparation with high purity and high homogeneity [6–8]. Energy-transfer and frequency up-conversion in Ho^{3+} and Er^{3+} ions-doped $BaTiO_3$ and many other rare earth doped BT materials for up-conversion application were described previously [9–13]. In contrast however, much fewer works have appeared on the up-conversion of Nd^{3+} ions-doped nano-crystalline $BaTiO_3$, which provide emission of radiation at higher energy than the excitation wavelength. For this reason, we decided to discover the up-conversion of this material doped with Nd^{3+} ions.

The objective of the present work is to develop nano-structured ferroelectric pure BT and BT doped with Nd^{3+} ions, with different concentrations, in the form of powder materials by using sol–gel technique. Structural characterizations carried out using FTIR and XRD. The tetragonal phase of the prepared samples will be detected using XRD analysis and their crystal sizes were determined using the peak profile.

We will report and discuss the up-conversion luminescence under the excitation of 808 nm laser diode for the powder derived Nd^{3+} ions doped the mentioned nano-structure BT materials.

* Corresponding author. Tel.: +2 02 25194104/0101526515; fax: +20 233370931.
E-mail address: szbasha@yahoo.com (I.K. Battisha).

0925-8388/$ – see front matter © 2009 Elsevier B.V. All rights reserved.
doi:10.1016/j.jallcom.2009.09.021

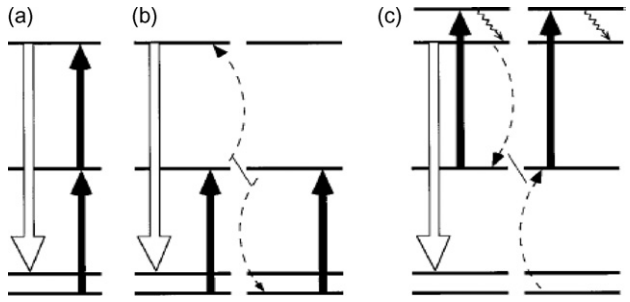

Fig. 1. The three basic mechanisms of up-conversion: (a) multi-photon absorption, (b) energy-transfer up-conversion, and (c) the photon avalanche mechanism.

2. Experimental

2.1. Powders preparation

$BaTiO_3$ (BT) doped with different concentrations 1, 3 and 5 mol % of $Nd^{3+}(NO_3)_3$, (BT1Nd, BT3Nd and BT5Nd), respectively, in powder form were prepared by a modified sol–gel method. Barium acetate ($Ba(Ac)_2$) and titanium butoxide ($Ti(C_4H_9O)_4$) were used as the starting materials; acetyl acetone ($AcAc,C_5H_8O_2$), acetic acid (HAc)–H_2O mixture were adopted as solvents of Ti ($C_4H_9O)_4$ and $Ba(Ac)_2$, respectively. $Nd(NO_3)_3$–H_2O solution were added to the precursor with different molar ratios of Nd^{3+} ions, respectively. The sol kept in air at room temperature, yielding transparent solution. The dry gel obtained by baking the gel at about 130 °C, and then annealed at 750 °C for 30 min to form nano-structure powder BT doped with Nd^{3+} ions, respectively.

2.2. Characterization

X-ray diffraction (XRD) patterns of the prepared samples were recorded with a Philips X-ray diffractometer using mono-chromatized $CuK_{\alpha 1}$ radiation of wavelength · = 1.54056 Å from a fixed source operated at 45 kV and 9 mA. Crystallite sizes G were determined from the Scherrer's equation ($G = K\lambda/D\cos\theta$), where K is the Scherrer constant (0.89), λ is the diffraction for a particular Bragg diffraction peak, and D is the (corrected) full width (in radians) of the peak at half-maximum (FWHM) intensity. The correction to the measured FWHM Ds for a sample peak made to accommodate systemic instrumental broadening and utilized peak widths Dq measured from a diffraction scan, taken under identical conditions, from a strain-free powdered quartz sample, with crystallite size ranging between 5 and 10 μm. The corrected sample peak widths were calculated as $D = (Ds^2 - Dq^2)^{1/2}$, where Ds is the full width of the peak at its half-maximum (FWHM) intensity of the prepared sample and Dq is of the standard quartz sample. Micro-strain and crystallite size contributions to D separated using the Win-Fit program, using standard samples for estimation of instrumental broadening. The final sample crystallite sizes G obtained by Fourier analysis, using the corrected profile. The diffraction peak used was the most intense diffraction peak, assigned to the (1 1 0) reflection from the BT powder phase.

The infrared spectrophotometer used was Mattson 1000 series LC operating. Issue I (0791) spectrophotometer.

The excitation and up-conversion emissions spectra of the prepared samples were recorded using laser diode at 808 nm. Incident beam power was 300 mW. The emission analyzed by Acton Spectra Pre 500 double monochromator (Gratting 1200) and detected with a photon counter. The PL emission obtained using lock-in amplifier (SR 510-Stanford) technique and recorded by computer. The measurements performed at room temperature.

3. Results and discussions

3.1. XRD analysis of pure BT and BT doped with different Nd^{3+} ion concentrations

Fig. 2 shows the XRD patterns of pure BT in powder form and sintered at heat treatment temperature 750 °C for 1 h. It seen that crystallized BT phase can be obtained at heating temperature 750 °C, indicating that one phase, tetragonal BT is presented in the prepared pure samples. It is evident that peaks at $2\theta = 22.18$, 31.7, 38.9, 45.26, 50.88, 56.27, 65.9, 70.5, 74.87, and 79.23° indexed as (1 0 0), (1 1 0), (1 1 1), (0 0 2), (2 1 0), (2 1 1), (2 2 0), (3 0 0), (3 1 0), and (3 1 1) diffraction line of tetragonal phase appeared, respectively.

The influence of the Nd^{3+} ions content on the BT powder structure can be observed in Fig. 3, this figure illustrates the XRD patterns for the BT powders with the addition of different concentrations of Nd^{3+} ions. The obtained BT phase for the pure and doped samples have a tetragonal perovskite structure, (By reference to JCPDS files 75-0215 and 79-2265 for tetragonal phases for pure and doped samples, respectively). This present phase is evident from the splitting of the (0 0 1) and (1 0 0) doublets, with an un-wanted amount of $BaCO_3$ (By reference to JCPDS files 45-1471 and 71-2394 for Witherite, syn $BaCO_3$ for pure and doped samples), respectively. This produced from the reaction of BaO with atmospheric CO_2 and the burnout of organic materials or from the incomplete calcinations. No other detectable secondary phases were found in the pure BT. While due to the solubility of Nd_2O_3, the doping with different concentrations caused secondary phase or impurity phase of $Nd_2Ti_2O_7$ at $2\theta = 27.66$, 33.7 and 34.58 indexed as (0 0 4), (2 0 4) and (1 2 0), as shown in Fig. 3, respectively.

The analysis of the XRD patterns indicate that the splitting in the (0 0 1) and (1 0 0) doublets decreases with the increase of Nd^{3+} ions concentration indicating a gradual transition from the tetragonal to the cubic phase and hence a lowering in the tetragonality factor can be observed, this result is in agreement with the previously reported by Yao et al., who studied the Raman spectra beside the XRD to confirm that, the Raman intensity of doped $BaTiO_3$ gradually decreased and the peaks became weaker and broader indicative of some structural reordering taking place such as tetragonal to cubic phase transition [14]. It is evidence from Table 1 that by increasing the Nd^{3+} ions content the crystallite sizes decreases.

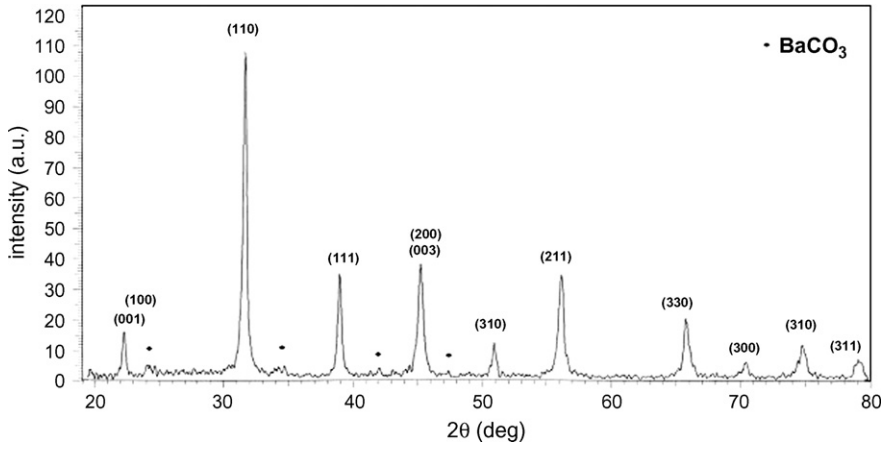

Fig. 2. XRD patterns of pure nano-structure BT powder sample sintering for 1 h at 750 °C.

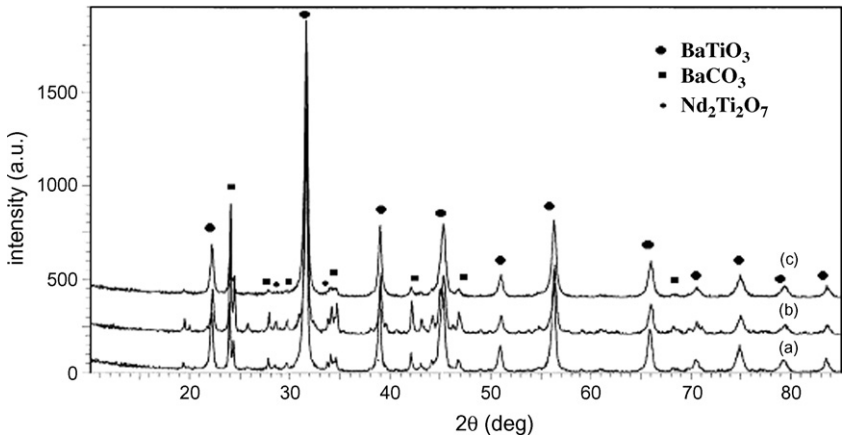

Fig. 3. XRD patterns of nano-structure BT powder doped with different concentrations of Nd^{3+} ions (a) (BT1Nd), (b) (BT3Nd) and (c) (BT5Nd).

Table 1
The effect of increasing the Nd^{3+} ions concentration on the crystallite size of the doped BT powder with different concentrations of Nd^{3+} ions, (BT1Nd), (BT3Nd) and (BT5Nd).

Crystallite size (nm)	Dopant name
39	BT1Nd
34	BT3Nd
30	BT5Nd

3.2. FTIR studies

3.2.1. FTIR spectra of pure nano-structure BT

Fig. 4 shows the FTIR spectra of pure nano-structure BT. The small band at 3389 cm^{-1} corresponds to the symmetric and asymmetric stretching vibrations of weakly bound water interacting with its environment via hydrogen bonding and to stretching vibrations of hydrogen-bonded OH groups [15,16]. The bands at 2921, 2854 and 2390 cm^{-1} assigned to the adsorption of CH_2 groups. The 1642 cm^{-1} band, (bending mode of H_2O) indicates that some H_2O is present, The strong absorption peak at 1434 cm^{-1} is due to the asymmetric stretching of the carbonates ion impurities ($BaCO_3$), detected in Section 3.1. of the XRD analysis. The peaks at 858 and 1751 cm^{-1} are also characteristic of the (CO_3) group. It is well known that hydrogen impurities can penetrate several ternary oxides with perovskite structure as H^+ bonded to lattice oxygen in the form of an OH^-. These protons can compensate for the cation charge defect due either to reduced centers such as trivalent dopants or to cation vacancies in nonstoichiometric samples. The band at 405 cm^{-1} is due to metal–oxygen bonds [17]. The broad band at 530 cm^{-1} is typical of the Ti–O vibrations in $BaTiO_3$.

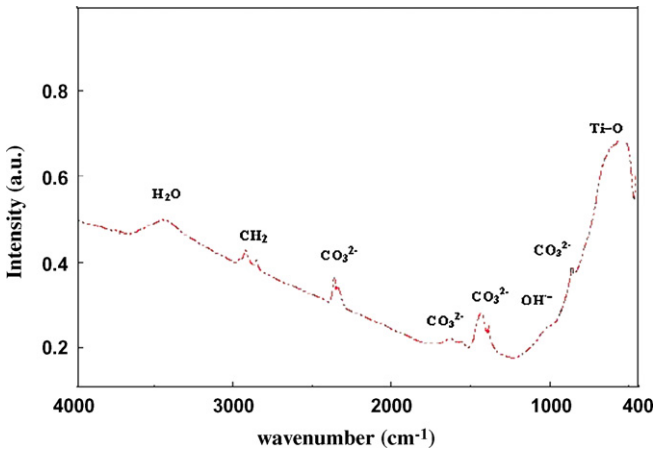

Fig. 4. FTIR spectra of pure nano-structure BT powder.

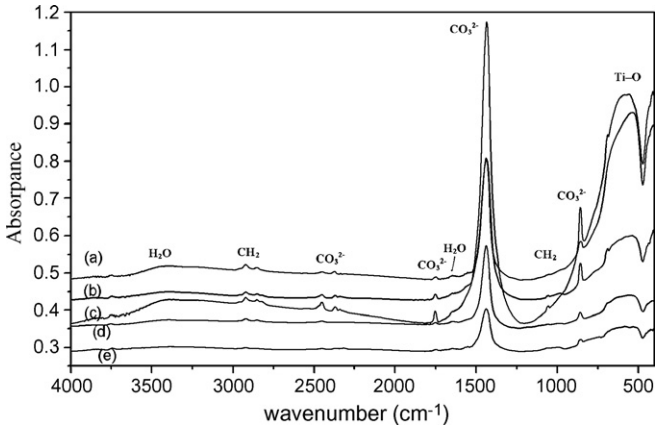

Fig. 5. FTIR spectra of nano-structure BT (a) BT1Nd, (b) BT2Nd, (c) BT3Nd (d) BT4Nd and (e) BT5Nd.

3.2.2. FTIR spectra of Nd^{3+} ions embedded BT

Fig. 5 shows the FTIR spectra of nano-structure BT doped with different concentrations of Nd^{3+} ions. The low-frequency region of the spectrum at 988 cm^{-1} attributed to O–H bonded to titanium for samples containing Nd^{3+} ions, it decreases by increasing the dopant content. The same trend of the 988 cm^{-1} band obtained in the strong absorption peak of asymmetric stretching carbonates ion ($BaCO_3$) at 1434 cm^{-1},which shifted to higher wave number by increasing the Nd^{3+} ions content, this might be explained due to the replacement of Ba^{2+} by Nd^{3+} ions. The influence of the replacement on the interaction between Ti and O can be observed by investigating the absorption peak of the Ti–O bond at 534 cm^{-1} which, shifted to higher wave number at 552 cm^{-1}, decreased in intensity and become broader by increasing the content of Nd^{3+} ions. It is attributed to the decrease of the unit cell volume as detected in Section 3.1 of the XRD analysis. The length of Ti–O bond is shortened by replacement of Nd^{3+} ions, then the interaction between Ti and O is enhanced which confirms the XRD analysis [18,19].

3.3. Up-conversion emission of Nd^{3+} ions-doped nano-structure BT powder

The excited state absorption (ESA) corresponding to the visible emissions of Nd^{3+} ions embedded in nano-structure BT powder

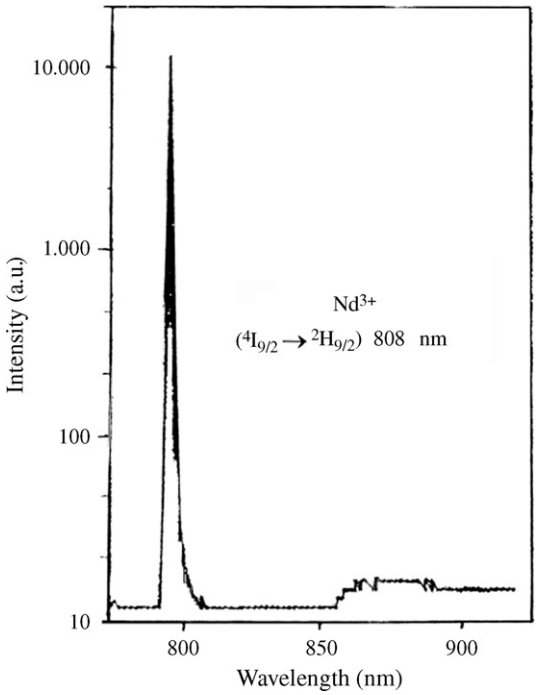

Fig. 6. The excited state absorption (ESA) corresponding to the visible emissions of Nd^{3+} ions embedded in nano-structure BT powder upon excitation at 808 nm.

upon excitation at 808 nm is shown in Fig. 6. The absorption in the range from 790 to 810 nm assigned to $(^4I_{9/2} \rightarrow {}^4H_{9/2})$ indicates that the laser diodes operating at 808 nm are the efficient pump sources for the green and NIR up-conversion emission.

The up-conversion emission spectra of nano-structure BT doped with different Nd^{3+} ions concentrations under excitation at 808 nm is shown in Fig. 7. Two major up-converted bands observed at ~533 nm (green) and ~635 nm (red) originated from the $^4G_{7/2} \rightarrow {}^4I_{9/2}$ and $^4G_{7/2} \rightarrow {}^4I_{13/2}$ transitions, respectively. The intensity of these two increases by increasing the Nd^{3+} ions content, while green concentration quenching commences to appear BT5Nd at 533 nm. In addition to these bands very weak emission bands also appear at 608 and 515 nm due to $^4G_{7/2} \rightarrow {}^4I_{11/2}$ and $^4G_{11/2} \rightarrow {}^4I_{11/2}$ transitions, respectively. Beside another very weak emission band at 457 nm attributed to the transition $(^2D_{5/2} \rightarrow {}^4I_{9/2})$.

A combination of two mechanisms such as excited state absorption (ESA) and energy transfer (ET) as sketched in Fig. 8 can explain the observed mechanism of the up-conversion emissions.

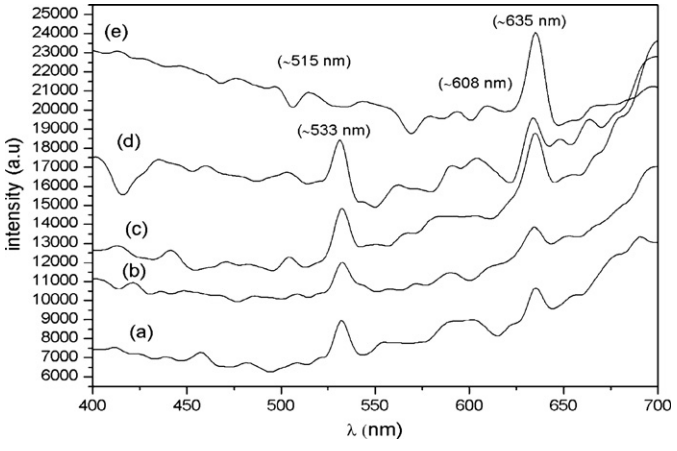

Fig. 7. Up-conversion emission spectra (under 808 nm excitation) from (a) BT1Nd, (b) BT2Nd, (c) BT3Nd, and (d) BT4Nd.

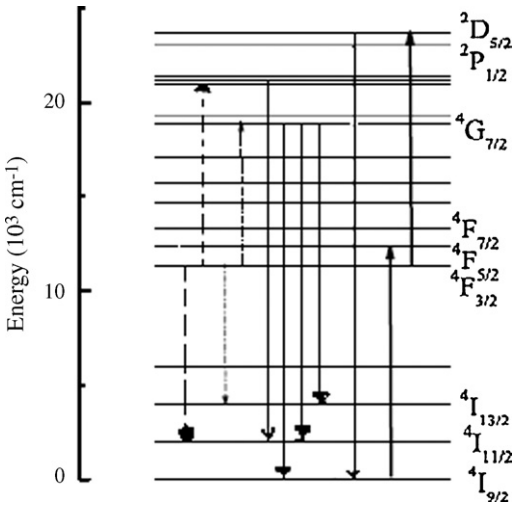

Fig. 8. Energy levels diagram of the up-converted transitions of Nd^{3+} ions incorporated into nano-structure BT.

The efficiency of ESA is independent on Nd^{3+} ions concentration, since it involves only one active ion, it is expected that ESA would be the dominant mechanism at low concentration of active ions. In the ESA process, the absorption of the first pump photon (808 nm) by a Nd^{3+} ion in the ground state absorption (GSA) initially excites it to the $^4F_{5/2}$ energy level of the same ion. There is non-radiative multiphonon relaxation from the metastable $^4F_{5/2}$ level to the $^4F_{3/2}$ level, which has a comparatively greater lifetime (stability) than $^4F_{5/2}$ levels; In fact the rate of multiphonon relaxation from $^4F_{5/2}$ to $^4F_{3/2}$ level is so high that every electron is expected to immediately relax to $^4F_{3/2}$ level. Thus, population ultimately grows in the $^4F_{3/2}$ level, which will increase the possibility of absorbing another 808 nm pump photon by exciting it to the $^2D_{5/2}$ level (ESA). Also it relaxes non-radiatively to the lower $^4G_{7/2}$ level in the order: $^4I_{9/2} \rightarrow {}^4F_{5/2}$ (GSA) $\rightarrow {}^4F_{3/2}$ (NR) $\rightarrow {}^2D_{5/2}$(ESA) $\rightarrow {}^4G_{7/2}$ (NR) or relaxes radiatively to the $^4I_{9/2}$ state emitting 457 nm photon. The emission spectrum of trivalent neodymium (Nd^{3+}) dominated by the radiative transitions from the $^4G_{7/2}$ excited level to $^4I_{9/2}$ and $^4I_{13/2}$ levels. The excited Nd^{3+} ions of the $^4F_{3/2}$ level transfers energy to another neighboring excited Nd^{3+} ion of the same level according to the resonant channels of $(^4F_{3/2}, {}^4F_{3/2}) \rightarrow (^4I_{13/2}, {}^4G_{7/2})$ and return to the ground state, whereas the second ion after receiving the energy, transit upward to the $^4G_{7/2}$ state. Another ET mechanism can occur through the following resonant channel $(^4F_{3/2}, {}^4F_{3/2}) \rightarrow (^4I_{11/2}, {}^2G_{9/2})$ [20,21]. Thus, ET occurs between two Nd^{3+} ions in $^4F_{3/2}$ level thereby one is excited to $^2G_{9/2}$ level and another ion return to the lower $^4I_{11/2}$ state. Such excitation of ET results in higher population of $^4G_{7/2}$ energy emitting levels. Another possible mechanism for the enhanced population of $^4G_{11/2}$ and $^4G_{7/2}$ levels may be the ET between two nearby Nd^{3+} ions. Two excited Nd^{3+} ions at $^2D_{5/2}$ and $^4F_{3/2}$ levels interacted with each other by resonant cross-relaxation (RCR) of $^2D_{5/2} \rightarrow {}^4G_{11/2}$ and $^4F_{3/2} \rightarrow {}^4F_{7/2}$, thereby populating the metastable $^4G_{11/2}$ state.

Considering the enormous intensity of the 635 nm red emission band compared to the 533 nm green one, it is reasonable to presume that transitions from some additional state also participates in addition to the $^4G_{7/2} \rightarrow {}^4I_{13/2}$ transition to bring about the enhanced red emission. This may be the $^2G_{9/2}$ and $^4G_{11/2}$ states. The $^2G_{9/2}$ level is populated by ET process while the $^4G_{11/2}$ state is populated by cross-relaxation process. Higher Nd^{3+} concentration induces large crystal field splitting $^4G_{11/2}$, $^2G_{9/2}$ and $^4G_{7/2}$ states, reducing their separations. Radiative transitions from the $^2G_{9/2}$ and $^4G_{11/2}$ states to the terminal $^4I_{15/2}$ state $(^2G_{9/2} \rightarrow {}^4I_{15/2})$ and $^4G_{11/2} \rightarrow {}^4I_{15/2})$ overlaps with the $^4G_{7/2} \rightarrow {}^4I_{13/2}$ red transition thereby enhancing its intensity.

4. Conclusion

In this work we studied the influence of the Nd^{3+} ions content on the structure and the visible up-conversion luminescence properties of nano-structure $BaTiO_3$ studied.

Pure BT powder and doped with different concentration of Nd^{3+} ions, were successfully synthesized via sol–gel technique. Sintering of the prepared samples at 750 °C for one hour resulted in tetragonal phases, as confirmed by XRD analysis. Structural study revealed that the crystallite sizes were 39, 34 and 30 nm by increasing the Nd^{3+} ions content. It is obvious that the formation of $BaCO_3$ appears in the pure sample and increases in the doped samples.

Efficient infrared-to-visible conversion in the prepared samples observed, using 808 nm laser diode as excitation source, and its origin investigated. Two major up-converted bands were observed to be centered at ~533 nm (green) and ~635 nm (red) originated from the $^4G_{7/2} \rightarrow {}^4I_{9/2}$ and $^4G_{7/2} \rightarrow {}^4I_{13/2}$ transitions, respectively. In addition to these bands a very weak emission bands also appeared at 608 and 515 nm attributed due to $^4G_{7/2} \rightarrow {}^4I_{11/2}$ and $^4G_{11/2} \rightarrow {}^4I_{11/2}$ transitions, respectively.

References

[1] S.F. Lim, R. Riehn, W.S. Ryu, N. Khanarian, C. Tung, D. Tank, R.H. Austin, Nano Lett. 6 (2) (2006) 169–170.
[2] K. Kuningas, T. Rantanen, T. Ukonaho, T. Lovgren, T. Soukka, Anal. Chem. 77 (2005) 7348–7355.
[3] Y. Li, G. Hong, Y. Zhang, Y. Yu, J. Alloys Comp. 456 (2008) 247–250.
[4] X. Li, Q. Nie, S. Dai, T. Xu, L. Lu, X. Zhang, J. Alloys Comp. 454 (2008) 510–514.
[5] W.P. Risk, T.R. Gosnell, A.V. Nurmikko, Compact Blue-Green Lasers, 1st ed., Cambridge University Press, 2003 (Ch. 7).
[6] K.C. Verma, R.K. Kotnala, M.C. Mathpal, N. Thakur, P. Gautam, N.S. Negi, Mater. Chem. Phys. 114 (2009) 576–579.
[7] F. Zheng, M. Shen, L. Fang, X. Wu, W. Cao, Mater. Res. Bull. 44 (2009) 803–806.
[8] X. Wang, H. Liu, B. Yan, J. Eur. Ceram. Soc. 29 (2009) 1183–1187.
[9] I.K. Battisha, Y. Badr, A.G. Abed El Fatah, Int. J. Mater. Sci. IJoMS 3 (2) (2008) 95–103.
[10] I.K. Battisha, J. Sol–Gel Sci. Technol. 30 (2004) 163–173.
[11] H.X. Zhang, C.H. Kam, Y. Zhou, X.Q. Han, Y.L. Lam, Y.C. Chan, K. Pita, Mater. Chem. Phys. 2 (2000) 174–177.
[12] H.X. Zhang, C.H. Kan, Y. Zhou, X.Q. Han, S. Buddhudu, Q. Xiang, Y.L. Lam, C.W. Chan, Appl. Phys. Lett. 77 (5) (2000) 609–611.
[13] M.S. Zhang, J. Yu, W.C. Chen, Z. Yin, Prog. Cryst. Growth Charact. Mater. 40 (1–4) (2000) 33–34.
[14] Z. Yao, H. Liu, Z. Wu, Z. Shen, Y. Liu, M. Cao, J. Mater. Chem. Phys. 109 (2008) 475.
[15] M. Stockenhuber, H. Mayer, J.A. Lercher, J. Am. Ceram. Soc. 76 (5) (1993) 1185–1190.
[16] L. Weidong, Li. Jiazhi, G. Jingkun, J. Eur. Ceram. Soc. 23 (2003) 2289–2295.
[17] Y.M. Baikov, E.K. Shalkova, J. Solid State Chem. 97 (1992) 224.
[18] X. Jin, D. Sun, M. Zhang, Y. Zhu, J. Qian, J. Electroceram. 22 (2009) 285.
[19] Y. Jung, D. Lim, J. Nho, S. Cho, R.E. Riman, B.W. Lee, J. Cryst. Growth 274 (2005) 638.
[20] I.K. Battisha, J. Non Cryst. Solids 353 (2007) 1748.
[21] D. Wang, J. Luo, J. Yu, J. Liu, Q. Wang, Y. Guo, M. Yin, W. Zhang, S. Xia, J. Alloys Comp. 399 (2005) 57.